Characterization of laser wakefield acceleration efficiency with octave spanning near-IR spectrum measurements

M. J. V. Streeter,[1,2,3,4,*] Y. Ma,[5,1,2] B. Kettle,[3] S. J. D. Dann,[1,2] E. Gerstmayr,[3] F. Albert,[6] N. Bourgeois,[7] S. Cipiccia,[8] J. M. Cole,[3] I. Gallardo González,[9] A. E. Hussein,[5,10] D. A. Jaroszynski,[11,1] K. Falk,[12,13,14] K. Krushelnick,[5] N. Lemos,[6] N. C. Lopes,[3,15] C. Lumsdon,[16] O. Lundh,[9] S. P. D. Mangles,[3] Z. Najmudin,[3] P. P. Rajeev,[7] R. Sandberg,[5] M. Shahzad,[11,1] M. Smid,[12] R. Spesyvtsev,[11,1] D. R. Symes,[7] G. Vieux,[11,1] and A. G. R. Thomas[5,1,2,†]

[1]*The Cockcroft Institute, Keckwick Lane, Daresbury, WA4 4AD, United Kingdom*
[2]*Physics Department, Lancaster University, Lancaster LA1 4YB, United Kingdom*
[3]*The John Adams Institute for Accelerator Science, Imperial College London, London, SW7 2AZ, United Kingdom*
[4]*School of Mathematics and Physics, Queen's University Belfast, Belfast BT7 1NN, United Kingdom*
[5]*Center for Ultrafast Optical Science, University of Michigan, Ann Arbor, Michigan 48109-2099, USA*
[6]*Lawrence Livermore National Laboratory (LLNL), P.O. Box 808, Livermore, California 94550, USA*
[7]*Central Laser Facility, STFC Rutherford Appleton Laboratory, Didcot OX11 0QX, United Kingdom*
[8]*Diamond Light Source, Harwell Science and Innovation Campus, Fermi Avenue, Didcot OX11 0DE, United Kingdom*
[9]*Department of Physics, Lund University, P.O. Box 118, S-22100, Lund, Sweden*
[10]*Department of Electrical and Computer Engineering, University of Alberta, 9211 116 Street NW Edmonton, Alberta, T6G 1H9, Canada*
[11]*SUPA, Department of Physics, University of Strathclyde, Glasgow G4 0NG, United Kingdom*
[12]*Helmholtz-Zentrum Dresden-Rossendorf, Bautzner Landstrasse 400, 01328 Dresden, Germany*
[13]*Technische Universitat Dresden, 01062, Dresden, Germany*
[14]*Institute of Physics of the ASCR, 182 21 Prague, Czech Republic*
[15]*GoLP/Instituto de Plasmas e Fusão Nuclear, Instituto Superior Técnico, Universidade de Lisboa, Lisboa 1049-001, Portugal*
[16]*York Plasma Institute, Department of Physics, University of York, York YO10 5DD, United Kingdom*

(Received 13 November 2020; accepted 12 September 2022; published 31 October 2022)

We report on experimental measurements of energy transfer efficiencies in a GeV-class laser wakefield accelerator. Both the transfer of energy from the laser to the plasma wakefield and from the plasma to the accelerated electron beam was diagnosed by simultaneous measurement of the deceleration of laser photons and the acceleration of electrons as a function of plasma length. The extraction efficiency, which we define as the ratio of the energy gained by the electron beam to the energy lost by the self-guided laser mode, was maximized at $19 \pm 3\%$ by tuning the plasma density and length. The additional information provided by the octave-spanning laser spectrum measurement allows for independent optimization of the plasma efficiency terms, which is required for the key goal of improving the overall efficiency of laser wakefield accelerators.

DOI: 10.1103/PhysRevAccelBeams.25.101302

Intense laser pulses can drive compact plasma-based electron accelerators using a process known as laser wakefield acceleration (LWFA). As the laser pulse propagates through a plasma, it drives electron oscillations that produce large electrostatic fields, typically of order 100 GV/m. LWFA has been successfully used to accelerate electrons to > 1 GeV energy levels over interaction distances on the order of a centimeter [1–6]. A crucial consideration for LWFAs is the efficiency of energy transfer from the laser to the accelerated particle bunch. In radio-frequency (rf) linear accelerators, efficient operation is achieved by storing the drive energy in a high-quality factor cavity, which is then extracted by multiple electron beams in a bunch train. In high-amplitude plasma accelerators, nonlinearities eventually damp out the plasma oscillations and so high-efficiency energy transfer

*m.streeter@qub.ac.uk
†agrt@umich.edu

must be achieved within a relatively small number of plasma oscillation periods.

In plasma accelerators, the driver energy is converted to the accelerating fields via the plasma response so that the total efficiency of the accelerator can be broken down as $\eta = (\eta_{\mathrm{AC}\to\mathrm{driver}}) \cdot (\eta_{\mathrm{driver}\to\mathrm{plasma}}) \cdot (\eta_{\mathrm{plasma}\to\mathrm{beam}})$, where the last term, from here on abbreviated as η_b, is the extraction efficiency. In beam-driven plasma wakefield acceleration (PWFA), the extraction efficiency is simply calculated as the ratio of the energy gained by the witness beam to the energy lost by the driver. Using this measure, an efficiency of $> 30\%$ has been observed experimentally [7]. In LWFA, energy transfer to the plasma wakefield occurs through redshifting of the driving laser pulse and so can be determined from spectral measurement of the postinteraction laser pulse [8,9]. Combined with the measurement of the accelerated electron beam spectrum, it is possible to simultaneously diagnose the efficiency with which the laser excites the plasma wakefield and the efficiency with which the electron beam extracts that energy. Higher-order laser modes that are not guided in a central filament will not drive strong plasma waves and therefore do not transfer significant energy to the wake [10]. Consequently, the extraction efficiency for LWFA only includes energy transfer from the guided and therefore redshifted, laser mode.

Regardless of the nature of the driver, 100% extraction efficiency would require that the wake of the witness beam perfectly cancels the plasma wake generated by the driver. With a suitably chosen trapezoidal electron beam current profile [11], the accelerating field over the electron bunch can be kept constant at $E_z(\xi_S)$, where ξ_S is the location of the head of the electron bunch in the comoving frame $\xi = z - ct$. Doing so allows for simultaneous high plasma wake extraction efficiency and low energy spread for the accelerated beam in linear [11] or nonlinear blowout [12–14] regimes. If dephasing occurs, then this ideal beam-loading condition can not be maintained, leading to increased energy spread and lower overall efficiency. Any modification to the wakefield amplitude, i.e., as the laser evolves, will affect both the ideal beam-loading condition and the dephasing rate.

In this paper, we present experimental measurements of the transfer of laser energy into a plasma wakefield and the efficiency with which that energy was extracted by an electron beam as it was accelerated to > 1 GeV. This required measurement of an extended spectral range of the shifted laser pulse at the exit of the plasma, which in this regime extended up to 1600 nm. Studying the energy transfer among the laser, plasma, and electron beam as a function of the plasma length was used to reveal the dynamics responsible for this optimum.

For the driving laser of an LWFA, assuming conservation of photon number (valid for $\Delta\omega < \omega_0$ and $\omega_p \ll \omega_0$ [15,16] and negligible levels of ionization or incoherent scattering), the energy loss per unit length is given by $-\mathrm{d}W_L/\mathrm{d}z = -(W_{L0}/\omega_0)\mathrm{d}\langle\omega\rangle/\mathrm{d}z$, where W_{L0} and ω_0 are the initial laser pulse energy and frequency, respectively. The electron-beam energy-gain per-unit-length, $N_B m_e c^2 d\langle\gamma\rangle/dz$, where N_B is the number of accelerated electrons and $\langle\gamma\rangle = \int S(\gamma)\mathrm{d}\gamma/N_B$ is the average energy of the beam, which can be inferred from measurements of the electron spectrum $S(\gamma)$ as a function of plasma length. Therefore, the instantaneous energy extraction efficiency for an LWFA can be written as

$$\tilde{\eta}_b = -\frac{N_B m_e c^2 \omega_0}{W_{L0}} \left[\frac{\mathrm{d}\langle\gamma\rangle}{\mathrm{d}z}\right] \left[\frac{\mathrm{d}\langle\omega\rangle}{\mathrm{d}z}\right]^{-1}. \tag{1}$$

Due to contributions by dephasing, drive laser evolution, beam injection, and beam loss (changing N_B), the extraction efficiency is not a constant but changes along the accelerator length. For the results of this paper, we measure the accelerator averaged extraction efficiency η_b, i.e., the ratio of the total energy gained by the electron beam to the energy lost by the laser pulse over the full acceleration length.

An experiment was performed (setup as shown in Supplemental Materials [17]) with the Gemini laser at the Central Laser Facility. Each pulse contained 6.3 ± 0.6 J in a pulse length of $\tau_{\mathrm{FWHM}} = 52 \pm 4$ fs, with a peak power of $P_0 = 113 \pm 19$ TW. The pulse had a positive chirp of 500 fs^2 compared to the shortest pulse length of 45 fs. The pulse was focused to a spot width of $50(\pm 2) \times 40(\pm 2)$ μm^2 ($x \times y$ FWHM) using an $f/40$ parabolic mirror and was linearly polarized along the x axis. A deformable mirror was used to optimize the wavefront, giving a peak intensity in a vacuum of $I_0 = 3.9(\pm 0.7) \times 10^{18}$ W cm^{-2} and a peak normalized vector potential $a_0 = 1.34 \pm 0.11$ at focus.

The laser pulse was focused into a 3D printed two-stage gas cell [18], filled with a 2%/98% nitrogen/helium mix for the first "injector" stage and pure helium in the second "accelerator" stage. The cell walls had 1-mm wide vertical slits to allow for the gas cell to be translated vertically. This enabled the accelerator length to be adjusted continuously as the exit wall was angled at 45 ° to the vertical plane. The injector stage has an internal length of 3 mm and the accelerator length was variable over 8–21 mm, giving a total gas cell length of 14–27 mm (including the cell boundaries). The electron density in the gas cells was varied in the range $n_e = 0$–2.6×10^{18} cm^{-3}, which was diagnosed by observing the spectrum of Raman side scattering from plasma waves generated by low intensity ($a_0 < 1$), long duration ($\tau_{\mathrm{FWHM}} \approx 200$ fs) laser pulses [19].

After interaction with the plasma, the transmitted laser pulse was reflected from two glass plates into a fiber coupler, sampling a 1-cm diameter region (1/10 of the full beam diameter at this point). A fiber splitter directed the signal onto two spectrometers, one measuring 350–840 nm (Andor Shamrock) and one measuring 900–1700 nm

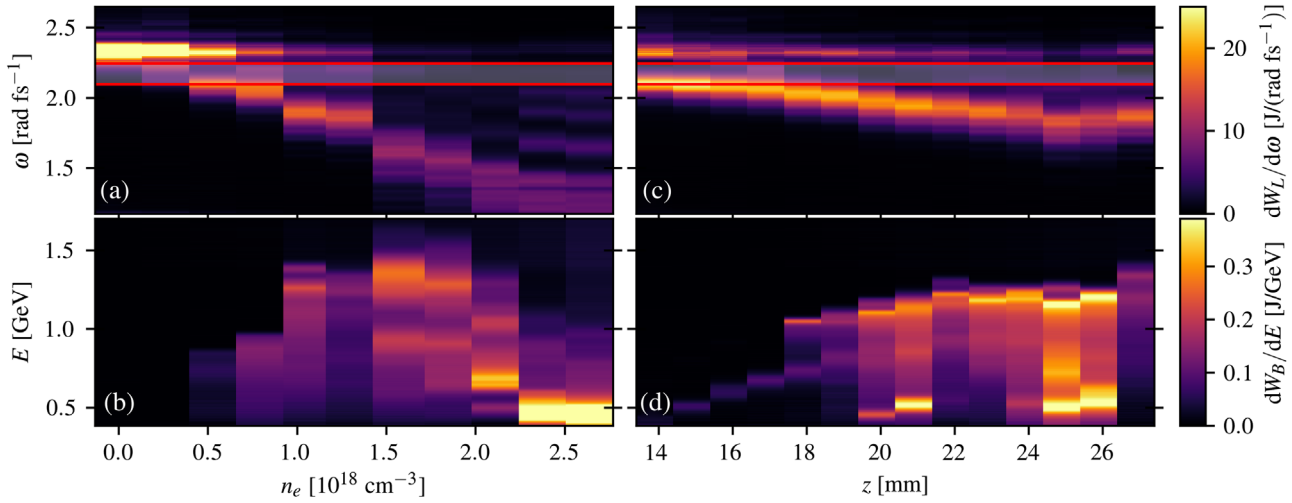

FIG. 1. Laser and electron spectrum at the exit of the 27-mm gas cell as functions of electron density (a) and (b) and as functions of accelerator stage length for $n_e = 1.25 \pm 0.06 \times 10^{18}$ cm^{-3} (c) and (d). The red-bordered region in the laser spectra plots indicates the gap between the measurement ranges of the two spectrometers, which was filled by interpolation. Each column of each image shows the average from three to five shots at the same conditions.

(Ocean Optics NIRQuest 512). The relative spectral sensitivities of the laser spectrometers were calibrated using a precalibrated white light source. The electron beam spectrum was measured using a magnetic dipole with integrated field strength $\int B\mathrm{d}z = 0.45$ Tm, which dispersed electrons in the energy range of 385–3000 MeV onto a Lanex scintillator.

In order to determine the optimal conditions for electron generation, the gas cell was positioned at its longest length and the plasma density n_e and longitudinal gas cell position were independently scanned. The results of the gas cell density scan, for an accelerator length of 21 mm (total plasma length of 27 mm), are plotted in Figs. 1(a) and 1(b).

The laser spectrum, shown in Fig. 1(a), was increasingly redshifted and broadened at higher plasma density. For the highest plasma density $n_e = 2.6 \times 10^{18}$ cm^{-3}, the laser spectrum extended to the limit of the spectrometer with a peak occurring at 1600 nm. Comparatively little laser energy was blueshifted for the full density range demonstrating that ionization blueshift and photon acceleration at the rear of the plasma wave were not significant [20].

As shown in Fig. 1(b), the highest electron energy occurred for $n_e = 1.5 \times 10^{18}$ cm^{-3}, where a peak in the spectrum was observed at 1.4 GeV. At higher densities, the maximum electron energies decreased, while the total measured charge remained approximately constant at $eN_B \approx 210$ pC. The increasing laser redshift indicates that a strong plasma wave continued to be driven at these high densities, but the injected electrons experienced less acceleration.

Figures 1(c) and 1(d) show the result of scanning the accelerator length for a fixed density of $n_e = 1.25 \times 10^{18}$ cm^{-3}. The laser Fig. 1(c) redshifted at an approximately linear rate as the acceleration length was increased. The electron spectra [Fig. 1(d)] shows two distinctive electron bunches were accelerated, with the higher energy component reaching 1.2 GeV. For plasma length $z < 18$ mm (acceleration cell length $z < 13$ mm), the charge in the higher energy component was much reduced, indicating that injection was sensitive to small changes in the plasma profile as the cell was translated vertically. Also for the longest plasma lengths ($z > 25$ mm), the laser redshift was reduced, indicating that less energy was coupled into the plasma. This was likely due to obstructions of the laser path at the top of the gas cell slits.

Both the laser and electron beam energies were calculated by integrating the measurements in Fig. 1 over the spectral axes. For the laser spectrum, there was a small gap between the ranges of the two spectrometers. In order to determine the interacting laser energy, Gaussian process regression (GPR) was used to fit the observed signal and interpolate over this region. The relative error of the interacting laser energy measurement introduced by this procedure was calculated from the GPR model uncertainties as less than 3% (standard deviation). Furthermore, the spectra were corrected to account for frequency dependent divergence of the source, using the assumption that all frequencies were emitted from a constant spot size. With this assumption, the divergence is inversely proportional to frequency and so the collection efficiency for an on-axis sample scales as ω^2 and so the corrected spectrum was obtained by dividing the measured spectrum by ω^2, i.e., $S_{\mathrm{cor}}(\omega) \propto S_{\mathrm{meas}}(\omega)/\omega^2$. Analysis of transmitted laser spectra from the PIC simulations (described later in this paper) indicates that this assumption leads to laser depletion being underestimated by ≈5%. Finally, it was assumed that the total photon number of the driving laser pulse ($N_{\mathrm{ph}} = W_{L0}/\hbar\omega_0$) was conserved throughout the

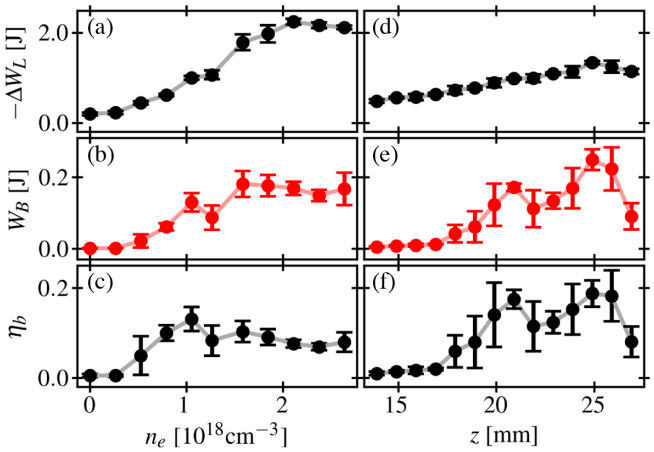

FIG. 2. Laser energy loss, electron beam energy, and extraction efficiency as functions of plasma density for $z = 27$ mm (a)–(c), and length (d)–(f) with $n_e = 1.25 \times 10^{18}$ cm^{-3}.

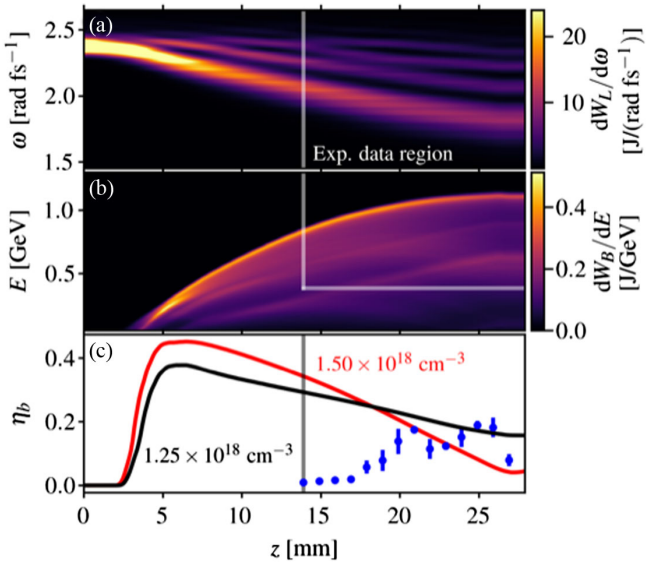

FIG. 3. (a) Laser and (b) electron spectra as functions of propagation distance taken from a PIC simulation with a plateau density of $n_e = 1.25 \times 10^{18}$ cm^{-3}. (c) The extraction efficiency, calculated as the ratio of the electron beam energy to the laser energy loss, for simulations with $n_e = (1.25, 1.5) \times 10^{18}$ cm^{-3} and the experimental measurements (blue points) at $n_e = 1.25 \times 10^{18}$ cm^{-3}.

interaction [8], such that the energy loss can be calculated from the change in average laser frequency as in Eq. (1).

The laser pulse energy loss and electron energy gain are plotted as functions of plasma density in Figs. 2(a) and 2(b). The laser lost more energy for increasing plasma density until reaching a plateau for $n_e > 1.6 \times 10^{18}$ cm^{-3}. The electron beam total energy reached a maximum of 0.18 ± 0.04 J at $n_e = 1.6 \times 10^{18}$ cm^{-3} and was lower for both higher and lower plasma densities. The extraction efficiency, $\eta_b = -W_B/\Delta W_L$, plotted in Fig. 2(c), reached a maximum of $13 \pm 3\%$ at $n_e = 1.05 \times 10^{18}$ cm^{-3}. Increasing the plasma density beyond this point resulted in lower extraction efficiency, even though the electron beam energy increased.

The laser energy loss and electron beam energy for the length scan are shown in Figs. 2(d) and 2(e). The laser energy loss was approximately linearly proportional to the plasma length up to $z = 25$ mm. The electron beam total energy increased suddenly with the appearance of the higher energy feature in the electron spectrum [visible in Fig. 1(d)], at $z = 18$ mm. Over the range $(20 \leq z \leq 26)$ mm, the electron charge had an average of $eN_B = 220 \pm 70$ pC, while the electron beam total energy increased with z. The extraction efficiency, shown in Fig. 2(f), also increased with the length for $z < 20$ mm as more charge was injected, before stabilizing at an average of $\eta_b = 16 \pm 3\%$ for $(20 \leq z \leq 26)$ mm with a maximum of $\eta_b = 19 \pm 3\%$. The maximum electron beam total energy was $W_b = 0.25 \pm 0.03$ J, giving a total LWFA efficiency $\eta_{\text{laser}\to\text{beam}} = 4.0 \pm 0.5\%$.

In order to explore the dynamics of the experiment, we performed quasi-3D PIC simulations using FBPIC [21], using four azimuthal modes (see details in Supplemental Material [17]). The laser pulse was initialized using the experimentally measured temporal profile and a Gaussian approximation to the measured focal spot energy distribution with an $a_0 = 1.34$. The simulation results matched the experimentally observed maximum electron energy and laser redshift, with relative differences of 5% and 0.1%, respectively. However, the simulated idealized laser pulse contained only 4.2 J of energy (66% of the laser energy in the experiment), indicating that the combination of laser pulse and target imperfections resulted in a lower proportion of the laser energy being guided than for a pure Gaussian mode, in-line with previous observations [10,22].

The laser and electron spectra, as functions of propagation distance within the PIC simulation, are shown in Figs. 3(a) and 3(b). The laser spectrum was seen to redshift and broaden by the same amount as the experimental measurements of Fig. 1(c), with a redshifted peak at $\omega = 1.9$ rad fs^{-1}. The laser reached a peak normalized vector potential of $a_0 = 3$ at $z = 4.4$ mm due to the effects of self-focusing and self-compression. For the rest of the accelerator, $a_0 < 3$ and no self-injection was observed. The accelerated electron beam resulted from the trapping of inner shell electrons from nitrogen (ionization injection [23–26]) during the first 5 mm. A total beam charge of 255 pC was observed in the accelerated beam at the end of the simulation, with a peak in the energy of 1.2 GeV. Approximately 16% of the electron beam energy at the end of the simulation lies below the 385 MeV detection threshold of the experimental spectrometer, indicating that the experimentally measured extraction efficiency is underestimated by a similar amount.

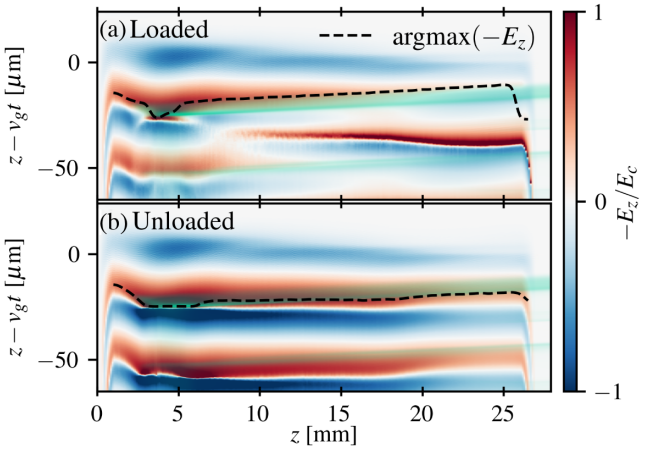

FIG. 4. (a) Loaded and (b) unloaded longitudinal electric field and injected electron bunch position (green) over the propagation axis z of PIC simulations with $n_e = 1.25 \times 10^{18}$ cm^{-3}. The unloaded fields were extracted from a simulation without the ionization injection species. The maximum accelerating field position in the first plasma period (black line) is overlaid.

The extraction efficiency is shown in Fig. 3(c) for $n_e = 1.25 \times 10^{18}$ cm^{-3} and for a slightly higher density $n_e = 1.5 \times 10^{18}$ cm^{-3}. For the higher density case, the laser intensity reached a larger value during the initial self-focusing, resulting in the trapping of ∼40% more charge. Also for the higher density, the laser pulse maintained $a_0 > 2.5$ over the full acceleration distance, thereby driving a higher amplitude wake. As a result, beam loading was less severe and so the extraction efficiency was initially higher than for the lower density case. However, for the higher density case, the efficiency dropped significantly throughout the accelerator, as the electron beam was dephased and started to decelerate for $z > 17$ mm.

Simulations using the same plasma profile with plateau densities of $n_e = (1.1, 1.2, 1.3, 1.4) \times 10^{18}$ cm^{-3} show that both the maximum final electron energy and extraction efficiencies were optimized for $n_e = 1.2 \times 10^{18}$ cm^{-3}. Operating the LWFA at a higher density but over a shorter length allows for higher efficiency but results in lower maximum electron energy.

Figure 4 shows the electron beam position relative to the axial longitudinal electric field in the lab frame with a Galilean coordinate transform to the linear group velocity of the laser $\xi = z - v_g t$. The fields are shown both with [Fig. 4(a)] and without [Fig. 4(b)] the contribution of the trapped electron bunch. After the initial self-focusing phase, the laser pulse a_0 steadily dropped from $a_0 = 2$ to $a_0 = 1.5$ at $z = 22$ mm, causing a gradual reduction in the wavelength of the wakefield λ_p. In addition, the shape of the wakefield smoothly changed from the saw-tooth profile of the highly nonlinear regime to a quasilinear sinusoidal profile, which also had the effect of moving the position of the peak accelerating field further forward. As shown in Fig. 4(b), these effects combined to balance the subluminal group velocity of the driving laser pulse and so the trapped highly relativistic electrons closely tracked the position of highest field strength. Figure 4(a) shows the effect of beam loading, which reduced the accelerating field experienced by the rear of the bunch to ≈15% of the value at the head.

During injection, the normalized vector potential reached a peak value of $a_0 = 3$, significantly above the threshold for ionization injection. Electrons injected at this point were trapped on *deep* orbits [26] in which electrons obtained the wakefield phase velocity $v = v_\phi$ significantly before the back of the wake and so never experienced the maximum accelerating wakefield. From this point on, a nonevolving laser driver would have caused the electron beam to dephase at $L_\phi = 14.5$ mm with a maximum energy of 800 MeV. However, the driver evolution acted to mitigate dephasing, resulting in the higher observed electron beam energy of 1.2 GeV.

Methods for accelerating electrons to energies beyond the dephasing limit have been explored, including nonuniform plasma profiles [27–30] or using alternative laser focusing geometries with spatiotemporal couplings [31–33]. Phase-locked LWFA dynamics in a constant density plasma have been observed in PIC simulations previously [34] although in that case it was attributed to pulse depletion. However, depletion increases the wakefield amplitude due to laser redshifting ($a_0 \propto \omega^{-1/2}$) and so this effect alone would actually increase the wakefield wavelength and cause the electron beam to dephase more rapidly. Here we show that through careful management of the laser evolution, it is possible to mitigate dephasing so that pulse depletion determines the electron energy limit for the accelerator.

In conclusion, we have measured the extraction efficiency for an LWFA, which reached a maximum of $19 \pm 3\%$, close to that previously observed in electron beam–driven PWFA [7]. The measurements indicated that only approximately 20% of the laser pulse energy was transferred to the plasma wakefield, with approximately one-third of the laser energy wasted due to a nonideal focal spot. The overall efficiency could therefore be increased by improving the spatial distribution of the laser pulse, as indicated by PIC simulations with a Gaussian distribution as well as previous studies on the effects of non-Gaussian focal spots [10]. Laser energy that remains after the interaction could possibly be recovered to further improve the total efficiency of an LWFA facility. For the highest plasma densities and longest interaction length, the laser pulse spectrum was observed to span a complete octave from 800 to 1600 nm. Further harnessing these effects may open up a route to relativistic intensity single cycled mid-IR laser pulses [35–37].

The data and analysis scripts are available at the online repository zenodo.org at [38].

We acknowledge support from the UK STFC core Grants No. ST/P002056/1 (Cockcroft Institute), No. ST/P000835/1, No. ST/P002021/1, and No. ST/V001639/1 (John Adams Institute), UK EPSRC (EP/J018171/1, EP/N028694/1), the European Union's Horizon 2020 research and innovation programme under grant agreement Laserlab-Europe (871124), the National Science Foundation (Grant No. 1804463) and the Air Force Office of Scientific Research (Grant No. FA9550-16-1-0121). F. A. acknowledges funding from the DOE Early Career research program (Fusion Energy Sciences SCW1575-1).

[1] W. P. Leemans, B. Nagler, A. J. Gonsalves, C. Tóth, K. Nakamura, C. G. R. Geddes, E. Esarey, C. B. Schroeder, and S. M. Hooker, GeV electron beams from a centimetre-scale accelerator, Nat. Phys. **2**, 696 (2006).

[2] S. Kneip *et al.*, Near-GeV Acceleration of Electrons by a Nonlinear Plasma Wave Driven by a Self-Guided Laser Pulse, Phys. Rev. Lett. **103**, 035002 (2009).

[3] C. E. Clayton, J. E. Ralph, F. Albert, R. A. Fonseca, S. H. Glenzer, C. Joshi, W. Lu, K. A. Marsh, S. F. Martins, W. B. Mori, A. Pak, F. S. Tsung, B. B. Pollock, J. S. Ross, L. O. Silva, and D. H. Froula, Self-Guided Laser Wakefield Acceleration beyond 1 GeV Using Ionization-Induced Injection, Phys. Rev. Lett. **105**, 105003 (2010).

[4] X. Wang *et al.*, Quasi-monoenergetic laser-plasma acceleration of electrons to 2 GeV, Nat. Commun. **4**, 1988 (2013).

[5] W. P. Leemans, A. J. Gonsalves, H.-S. Mao, K. Nakamura, C. Benedetti, C. B. Schroeder, C. Toth, J. Daniels, D. E. Mittelberger, S. S. Bulanov, J.-L. Vay, C. G. R. Geddes, and E. Esarey, Multi-GeV Electron Beams from Capillary-Discharge-Guided Subpetawatt Laser Pulses in the Self-Trapping Regime, Phys. Rev. Lett. **113**, 245002 (2014).

[6] A. J. Gonsalves *et al.*, Petawatt Laser Guiding and Electron Beam Acceleration to 8 GeV in a Laser-Heated Capillary Discharge Waveguide, Phys. Rev. Lett. **122**, 084801 (2019).

[7] M. Litos *et al.*, High-efficiency acceleration of an electron beam in a plasma wakefield accelerator, Nature (London) **515**, 92 (2014).

[8] E. Esarey, C. B. Schroeder, and W. P. Leemans, Physics of laser-driven plasma-based electron accelerators, Rev. Mod. Phys. **81**, 1229 (2009).

[9] S. Shiraishi, C. Benedetti, A. J. Gonsalves, K. Nakamura, B. H. Shaw, T. Sokollik, J. van Tilborg, C. G. R. Geddes, C. B. Schroeder, C. Tóth, E. Esarey, and W. P. Leemans, Laser red shifting based characterization of wakefield excitation in a laser-plasma accelerator, Phys. Plasmas **20**, 063103 (2013).

[10] J. Vieira, S. F. Martins, F. Fiúza, C. K. Huang, W. B. Mori, S. P. D. Mangles, S. Kneip, S. Nagel, Z. Najmudin, and L. O. Silva, Influence of realistic parameters on state-of-the-art laser wakefield accelerator experiments, Plasma Phys. Controlled Fusion **54**, 055010 (2012).

[11] T. Katsouleas, S. Wilks, P. Chen, J. M. Dawson, and J. J. Su, Beam loading efficiency in plasma accelerators, Part. Accel. **22**, 81 (1987).

[12] S. Gordienko and A. Pukhov, Scalings for ultrarelativistic laser plasmas and quasimonoenergetic electrons, Phys. Plasmas **12**, 043109 (2005).

[13] W. Lu, M. Tzoufras, C. Joshi, F. Tsung, W. Mori, J. Vieira, R. Fonseca, and L. Silva, Generating multi-GeV electron bunches using single stage laser wakefield acceleration in a 3D nonlinear regime, Phys. Rev. ST Accel. Beams **10**, 061301 (2007).

[14] M. Tzoufras, W. Lu, F. S. Tsung, C. Huang, W. B. Mori, T. Katsouleas, J. Vieira, R. A. Fonseca, and L. O. Silva, Beam Loading in the Nonlinear Regime of Plasma-Based Acceleration, Phys. Rev. Lett. **101**, 145002 (2008).

[15] S. V. Bulanov, I. N. Inovenkov, V. I. Kirsanov, N. M. Naumova, and A. S. Sakharov, Nonlinear depletion of ultrashort and relativistically strong laser pulses in an underdense plasma, Phys. Fluids B **4**, 1935 (1992).

[16] L. Oliveira e Silva and J. T. Mendonça, Kinetic theory of photon acceleration: Time-dependent spectral evolution of ultrashort laser pulses, Phys. Rev. E **57**, 3423 (1998).

[17] See Supplemental Material at http://link.aps.org/supplemental/10.1103/PhysRevAccelBeams.25.101302 for experimental setup, and additional details on the analysis methods and numerical simulations.

[18] A. E. Hussein *et al.*, Laser-wakefield accelerators for high-resolution x-ray imaging of complex microstructures, Sci. Rep. **9**, 3249 (2019).

[19] T. Matsuoka, C. McGuffey, P. G. Cummings, Y. Horovitz, F. Dollar, V. Chvykov, G. Kalintchenko, P. Rousseau, V. Yanovsky, S. S. Bulanov, A. G. R. Thomas, A. Maksimchuk, and K. Krushelnick, Stimulated Raman Side Scattering in Laser Wakefield Acceleration, Phys. Rev. Lett. **105**, 034801 (2010).

[20] J. Schreiber, C. Bellei, S. P. D. Mangles, C. Kamperidis, S. Kneip, S. R. Nagel, C. A. J. Palmer, P. P. Rajeev, M. J. V. Streeter, and Z. Najmudin, Complete Temporal Characterization of Asymmetric Pulse Compression in a Laser Wakefield, Phys. Rev. Lett. **105**, 235003 (2010).

[21] R. Lehe, M. Kirchen, I. A. Andriyash, B. B. Godfrey, and J.-L. Vay, A spectral, quasi-cylindrical and dispersion-free Particle-In-Cell algorithm, Comput. Phys. Commun. **203**, 66 (2016).

[22] S. P. D. Mangles, G. Genoud, M. S. Bloom, M. Burza, Z. Najmudin, A. Persson, K. Svensson, A. G. R. Thomas, and C.-G. Wahlström, Self-injection threshold in self-guided laser wakefield accelerators, Phys. Rev. ST Accel. Beams **15**, 011302 (2012).

[23] T. P. Rowlands-Rees, C. Kamperidis, S. Kneip, A. J. Gonsalves, S. P. D. Mangles, J. G. Gallacher, E. Brunetti, T. Ibbotson, C. D. Murphy, P. S. Foster, M. J. V. Streeter, F. Budde, P. A. Norreys, D. A. Jaroszynski, K. Krushelnick, Z. Najmudin, and S. M. Hooker, Laser-Driven Acceleration of Electrons in a Partially Ionized Plasma Channel, Phys. Rev. Lett. **100**, 105005 (2008).

[24] A. Pak, K. A. Marsh, S. F. Martins, W. Lu, W. B. Mori, and C. Joshi, Injection and Trapping of Tunnel-Ionized Electrons into Laser-Produced Wakes, Phys. Rev. Lett. **104**, 025003 (2010).

[25] C. McGuffey, A. G. R. Thomas, W. Schumaker, T. Matsuoka, V. Chvykov, F. J. Dollar, G. Kalintchenko, V. Yanovsky, A. Maksimchuk, K. Krushelnick, V. Y. Bychenkov, I. V. Glazyrin, and a. V. Karpeev, Ionization Induced Trapping in a Laser Wakefield Accelerator, Phys. Rev. Lett. **104**, 025004 (2010).

[26] M. Chen, E. Esarey, C. B. Schroeder, C. G. R. Geddes, and W. P. Leemans, Theory of ionization-induced trapping in laser-plasma accelerators, Phys. Plasmas **19**, 033101 (2012).

[27] A. Pukhov and I. Kostyukov, Control of laser-wakefield acceleration by the plasma-density profile, Phys. Rev. E **77**, 025401(R) (2008).

[28] E. Guillaume, A. Döpp, C. Thaury, K. Ta Phuoc, A. Lifschitz, G. Grittani, J. P. Goddet, A. Tafzi, S. W. Chou, L. Veisz, and V. Malka, Electron Rephasing in a Laser-Wakefield Accelerator, Phys. Rev. Lett. **115**, 155002 (2015).

[29] Y. Ma, D. Seipt, S. J. D. Dann, M. J. V. Streeter, C. A. P. Palmer, L. Willingale, and A. G. R. Thomas, Angular streaking of betatron X-rays in a transverse density gradient laser-wakefield accelerator, Phys. Plasmas **25**, 113105 (2018).

[30] J. D. Sadler, C. Arran, H. Li, and K. A. Flippo, Overcoming the dephasing limit in multiple-pulse laser wakefield acceleration, Phys. Rev. Accel. Beams **23**, 021303 (2020).

[31] A. Debus, R. Pausch, A. Huebl, K. Steiniger, R. Widera, T. E. Cowan, U. Schramm, and M. Bussmann, Circumventing the Dephasing and Depletion Limits of Laser-Wakefield Acceleration, Phys. Rev. X **9**, 031044 (2019).

[32] J. P. Palastro, J. L. Shaw, P. Franke, D. Ramsey, T. T. Simpson, and D. H. Froula, Dephasingless Laser Wakefield Acceleration, Phys. Rev. Lett. **124**, 134802 (2020).

[33] C. Caizergues, S. Smartsev, V. Malka, and C. Thaury, Phase-locked laser-wakefield electron acceleration, Nat. Photonics **14**, 475 (2020).

[34] W. Li, J. Liu, W. Wang, Z. Zhang, Q. Chen, Y. Tian, R. Qi, C. Yu, C. Wang, T. Tajima, R. Li, and Z. Xu, The phase-lock dynamics of the laser wakefield acceleration with an intensity-decaying laser pulse, Appl. Phys. Lett. **104**, 093510 (2014).

[35] M. J. V. Streeter *et al.*, Observation of Laser Power Amplification in a Self-Injecting Laser Wakefield Accelerator, Phys. Rev. Lett. **120**, 254801 (2018).

[36] Z. Nie, C. H. Pai, J. Hua, C. Zhang, Y. Wu, Y. Wan, F. Li, J. Zhang, Z. Cheng, Q. Su, S. Liu, Y. Ma, X. Ning, Y. He, W. Lu, H. H. Chu, J. Wang, W. B. Mori, and C. Joshi, Relativistic single-cycle tunable infrared pulses generated from a tailored plasma density structure, Nat. Photonics **12**, 489 (2018).

[37] Z. Nie, C.-H. Pai, J. Zhang, X. Ning, J. Hua, Y. He, Y. Wu, Q. Su, S. Liu, Y. Ma, Z. Cheng, W. Lu, H.-H. Chu, J. Wang, C. Zhang, W. B. Mori, and C. Joshi, Photon deceleration in plasma wakes generates single-cycle relativistic tunable infrared pulses, Nat. Commun. **11**, 2787 (2020).

[38] M. J. V. Streeter, Characterisation of laser wakefield acceleration efficiency with octave spanning near-IR spectrum measurements, Zenodo, 10.5281/zenodo.7188057 (2022)